Available online at www.sciencedirect.com

ScienceDirect

Green Energy & Environment 10 (2025) 1559−1567

www.keaipublishing.com/gee

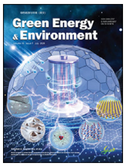

Research Paper

In situ converting the native passivation layer into a fast ion transport interphase to boost the stability of zinc anodes

Zi-Long Xie [a,b], Yunhai Zhu [c], Jia-Yi Du [a,b], Dong-Yue Yang [a,b], Hao Chen [a,b], Zhi Wang [a,b], Gang Huang [a,b,*], Xin-Bo Zhang [a,b,*]

[a] *State Key Laboratory of Rare Earth Resource Utilization, Changchun Institute of Applied Chemistry, Chinese Academy of Sciences, Changchun, 130022, China*
[b] *School of Applied Chemistry and Engineering, University of Science and Technology of China, Hefei, 230026, China*
[c] *State Key Laboratory of New Textile Materials and Advanced Processing Technologies, Wuhan Textile University, Wuhan, 430200, China*

Received 5 September 2024; revised 10 December 2024; accepted 10 February 2025
Available online 11 February 2025

Abstract

Aqueous zinc batteries offer significant potential for large-scale energy storage, wearable devices, and medium-to low-speed transportation due to their safety, affordability, and environmental friendliness. However, the uneven zinc deposition at the anode side caused by localized reaction activity from the passivation layer presents challenges that significantly impact the battery's stability and lifespan. In this study, we have proposed an expandable and maneuverable gel sustained-release (GSR) treatment to polish the Zn metal, which in situ converts its native passivation layer into a composite interphase layer with nanocrystal zinc phosphate and flexible polyvinyl alcohol. Such a thin and uniform interface contributes to fast and homogeneous Zn ion transport and improved anti-corrosion ability, enabling uniform zinc deposition without dendrite growth and thereby improving the battery performance with high-rate ability and long cycle life. This GSR treatment method, characterized by its simplicity, low cost, and universality, facilitates the widespread application of aqueous zinc batteries.

Keywords: Aqueous zinc batteries; Dendrite; Passivation layer; Interphase layer; Gel sustained-release treatment

1. Introduction

With the advantages of being non-flammable, cost-effective, and environmentally friendly, aqueous zinc batteries are promising candidates for diverse applications, particularly in large-grid energy storage [1]. Among the available anode materials, zinc metal stands out due to its high theoretical capacity, ease of recycling, and minimal processing steps compared to the ion-host anodes, like Mo_6S_8, TiS_2, etc [2–4]. However, the uneven deposition of zinc during cycling, which usually leads to serious dendrite growth [5−8], challenges the practical application of Zn anodes. Especially, the Zn dendrite growth induced soft short circuits and even direct battery failure significantly impacts the stability and lifespan of batteries.

Zinc is reactive and readily oxidizes in the air, producing an uneven oxidation layer on the Zn metal anodes used in experimental research. This passivation layer could hinder the transport of zinc ions, preferentially causing zinc deposition to occur at the layer-damaged sites. Consequently, the localized zinc deposition leads to dendritic growth [9,10]. To address this, researchers have employed mechanical and chemical methods to polish the Zn metal [11−14]. However, these conventional methods only temporarily remove the passivation layer, as the polished Zn anode re-oxidizes once exposed to the air again. Even if the oxidized layer is entirely removed,

---

* Corresponding authors.
E-mail addresses: ghuang@ciac.ac.cn (G. Huang), xbzhang@ciac.ac.cn (X.-B. Zhang).

Peer review under the responsibility of Editorial Board of Green Energy & Environment

https://doi.org/10.1016/j.gee.2025.02.004

2468-0257/

new types of passivation layers, such as zinc hydroxyl sulfate, would form in the aqueous solutions [15–19]. These native or newly formed passivation layers still contribute to uneven zinc deposition, dendritic growth, and side reactions, leading to battery failure with a limited lifetime. Therefore, removing the oxidative passivation layer from zinc metal while preventing the formation of newly disadvantageous passivation layers is crucial yet challenging.

Herein, we have proposed a gel sustained-release (GSR) treatment that could in situ convert the native oxidation layer into a high ionic conductivity and corrosion-resistant interphase on the Zn surface, effectively preventing the formation of subsequent passivation layers. The GSR design focuses on controlling the reaction rate, uniformity, and coating growth by the sustained release of coating-forming components through the gel network. The structure, properties, and zinc deposition behavior of the well-constructed nanocrystal zinc phosphate-dominated composite interphase layer have been investigated in detail through experiments and theoretical calculations. Benefiting from the compositional and structural advantages, the constructed interphase could effectively enhance the zinc deposition kinetics, regulate uniform zinc deposition, and consequently achieve long-cycle stability for the Zn||MnO_2 batteries.

2. Results and discussion

2.1. Gel sustained-release treatment to remove the passivation layer

Aqueous zinc batteries typically use commercially available high-purity zinc foils as the anode. However, the zinc stored in the natural environment is covered with a passivation layer on the surfaces (Fig. S1), primarily composed of zinc oxide, and accompanied by basic zinc carbonate in humid conditions [9,20]. Like other metal foils, zinc foils are produced by rolling, cutting, and coiling. Surface abrasion would inevitably occur during the manufacturing and packaging transportation of zinc foils. These mechanical scratches and pits are much more obvious at the microscopic level on the surface of raw zinc (Fig. 1a and b) [21]. Then, the zinc deposition behavior was investigated after artificially damaging the passivation layer using the in situ optical microscopy. As shown in Fig. S2, specific marks are made on the zinc foil surface with fine forceps to disrupt the naturally formed passivation layer, and the zinc deposition is observed mainly at the marked sites. The zinc deposition and dissolution reactions occur preferentially at the surface-damaged areas of raw Zn (denoted as Raw Zn), leading to localized reaction activity and dendritic growth (Fig. 1c). This indicates that the native passivation layer renders the zinc electrode surface with local reactivity.

Polishing metal surfaces with sandpaper is a common method in traditional processing industries to remove the passivation layers [22,23]. Scanning electron microscopy (SEM) images of zinc polished by sandpaper (Polished Zn) show that the physical polishing leaves behind surface textures (Fig. 1d and e). The edges of these grooves are often fragmented, with many embedded metal particles. The textures could provide numerous nucleation sites for zinc deposition, thus distributing the zinc deposition across the entire electrode surface at the beginning of cycles [11]. However, the defects and enlarged surface area caused by the mechanical grinding would exacerbate the surface corrosion and hydrogen evolution reaction (HER), limiting the long-term operation of batteries (Fig. 1f). Chemical etching is another viable method to remove the metal passivation layer [24,25]. Acids typically dissolve oxides but may also corrode parts of the metals. SEM images (Fig. 1g and h) show the evolution of the morphology of zinc etched by the phosphoric acid solution (Etched Zn). Due to the rapid acid etching reaction rate with the zinc substrate, numerous bubbles are produced. The adsorption of bubbles on the zinc surface continues to affect the subsequent etching process, resulting in uneven etching with rough surfaces (Fig. 1g and h). It is noteworthy that the interfacial properties could influence the acid etching reaction. During the process, acid etching primarily occurs at damaged sites of the passivation layer, and the etching reaction activity is also influenced by the crystal faces, leaving deep holes on the zinc surface [13,26]. Additionally, acid etching increases the active surface area of zinc, which could boost the HER side reaction during the battery cycling process (Fig. 1i).

Considering the disadvantages of the polishing and chemical etching methods, removing the passivation layer gently and uniformly from zinc surfaces is necessary to avoid introducing additional surface defects. Additionally, a stable interphase layer needs to be formed to protect the zinc from HER-induced corrosion reaction [27–29]. Inspired by drug release mechanisms, we aimed to implement GSR treatment to elaborately control the reaction rate and area to transform the native passivation layer into a stable and uniformly ion-conductive interphase (Fig. 1l), enhancing the long-term cycling stability of zinc electrodes. To form a solid-phase interphase layer and effectively conduct zinc ions, phosphoric acid was chosen as the release component to create zinc phosphate with high zinc ion conductivity [30,31]. Also, polyvinyl alcohol (PVA) was selected to act as the gel network component. On the one hand, the gel network can behave as a physical sieve for solute diffusion, ensuring uniformity in interfacial reactions [32–34]. On the other hand, the diffusion of protons in aqueous solutions is highly dependent on the Grotthuss mechanism. In hydrogels, the hydrogen-bond network of water molecules can be disrupted, hindering fast proton hopping diffusion [35,36]. Additionally, the hydroxyl functional groups of the gel network can interact with solutes, reducing their diffusion rate [32]. Thus, a precipitation reaction occurs on the zinc surface to transform the passivation layer into a zinc phosphate-dominated ion-conductive interphase with the help of the benefits brought by the gel network (reaction 1 and 2), different from the only acid corrosion induced by phosphoric acid solution. As expected, the GSR-treated zinc (GSR-Zn) exhibits a more homogeneous surface

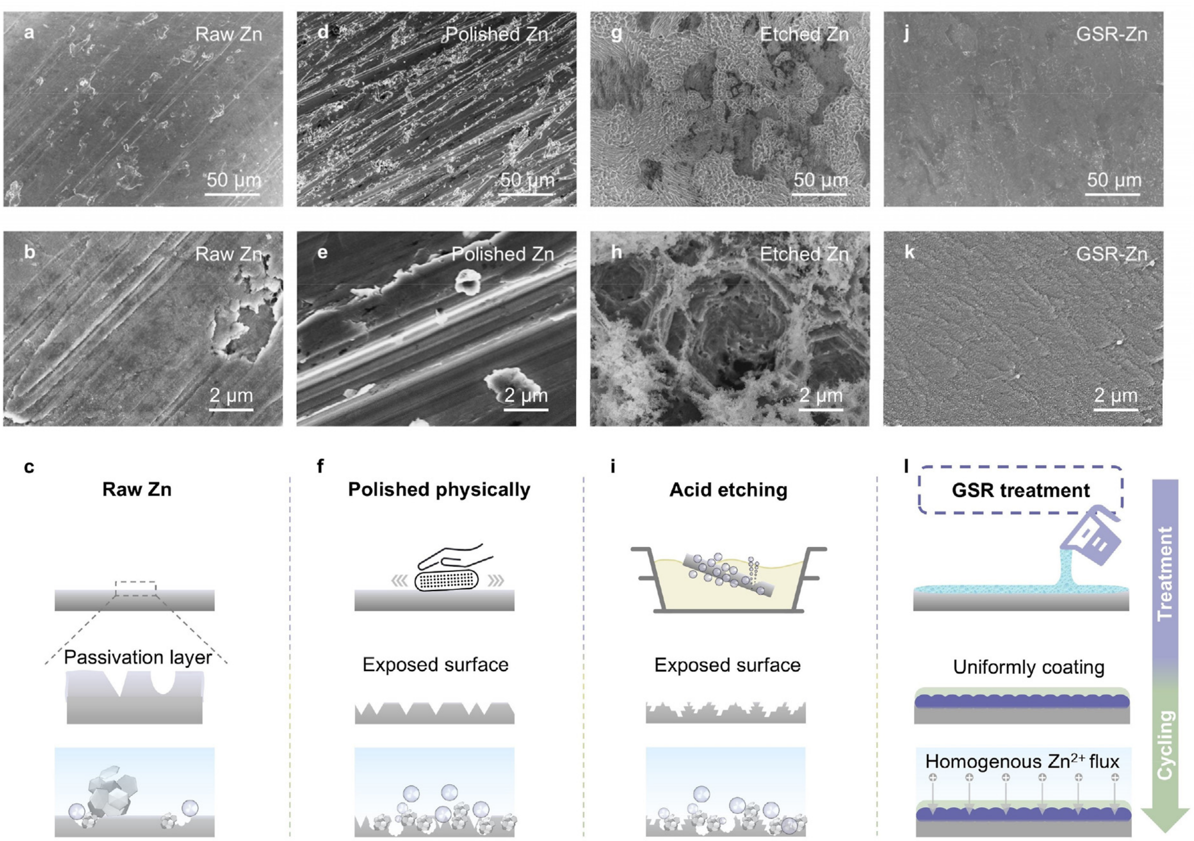

Fig. 1. Raw zinc and strategies to remove its passive layer. SEM images of Raw Zn (a, b), Polished Zn (d, e), Etched Zn (g, h), and GSR-Zn (j, k). Schemes of Raw Zn (c), Polished Zn (f), Etched Zn (i), and GSR-Zn (l).

morphology (Fig. 1j-l) than the zinc treated with other methods, which is beneficial for achieving uniform zinc deposition and preventing dendrite growth.

$$ZnO + H^{+} + PO_4^{3-} \rightarrow Zn_3PO_4 + H_2O \quad (1)$$

$$Zn + H^{+} + PO_4^{3-} \rightarrow Zn_3PO_4 + H_2\uparrow \quad (2)$$

2.2. Characterization of the zinc phosphate-dominated interphase layer

The optimized composition and structure of the well-designed zinc phosphate-dominated interphase layer were then detailly investigated. The surface morphology is confirmed to be a uniform layer of nanoscale particles through the SEM and atomic force microscopy (AFM) images (Fig. 2a and b). The image of the cross-section cut by a focused ion beam (FIB) shows that the thickness of the interphase layer is 60–80 nm (Fig. 2c). Energy dispersive spectroscopy (EDS) mapping of the cross-section (Fig. 2d) indicates that the granular interphase layer comprises Zn, P, and O elements, and the space between zinc phosphate particles is filled with O element, indicating the zinc phosphate particles homogeneously dispersed in the PVA gel matrix. Further confirmation of the phosphorus signal on the GSR-Zn was achieved through X-ray photoelectron spectroscopy (XPS) P 2p spectra (Fig. 2e). This proves that the GSR treatment is not simply acid etching but facilitates the formation of a solid zinc phosphate-rich interphase [37,38]. Raman spectra (Fig. 2f) reveal asymmetric vibration peaks from carbonate ions on the untreated zinc surfaces [39,40]. After GSR treatment, vibration peaks from phosphate ions [13,38] and C–H bonds appear on the zinc surface [41]. This demonstrates that the GSR treatment can effectively remove the surface passivation layer and in situ generate a composite interphase composed of nano-sized inorganic zinc phosphate and organic PVA gel. High-resolution transmission electron microscopy (HR-TEM) observation shows that the zinc phosphate particles are refined grains with a diameter of around 3 nm (Fig. 2g), approaching an amorphous state, with no diffraction peaks in the X-ray powder diffraction (XRD) pattern (Fig. S3). Such a nano-crystalline structure with abundant grain boundaries could effectively enhance the zinc ion diffusion capability [42–44]. In aqueous solutions, due to the fast reaction rate, crystalline zinc phosphate usually forms just within seconds [45]. For our GSR treatment, even after 1 h, only nano-crystalline zinc phosphate without diffraction peaks can be produced, demonstrating its ability to slow down the reaction rate, highlighting the advantage of the GSR treatment in promoting the construction of a uniform interphase layer.

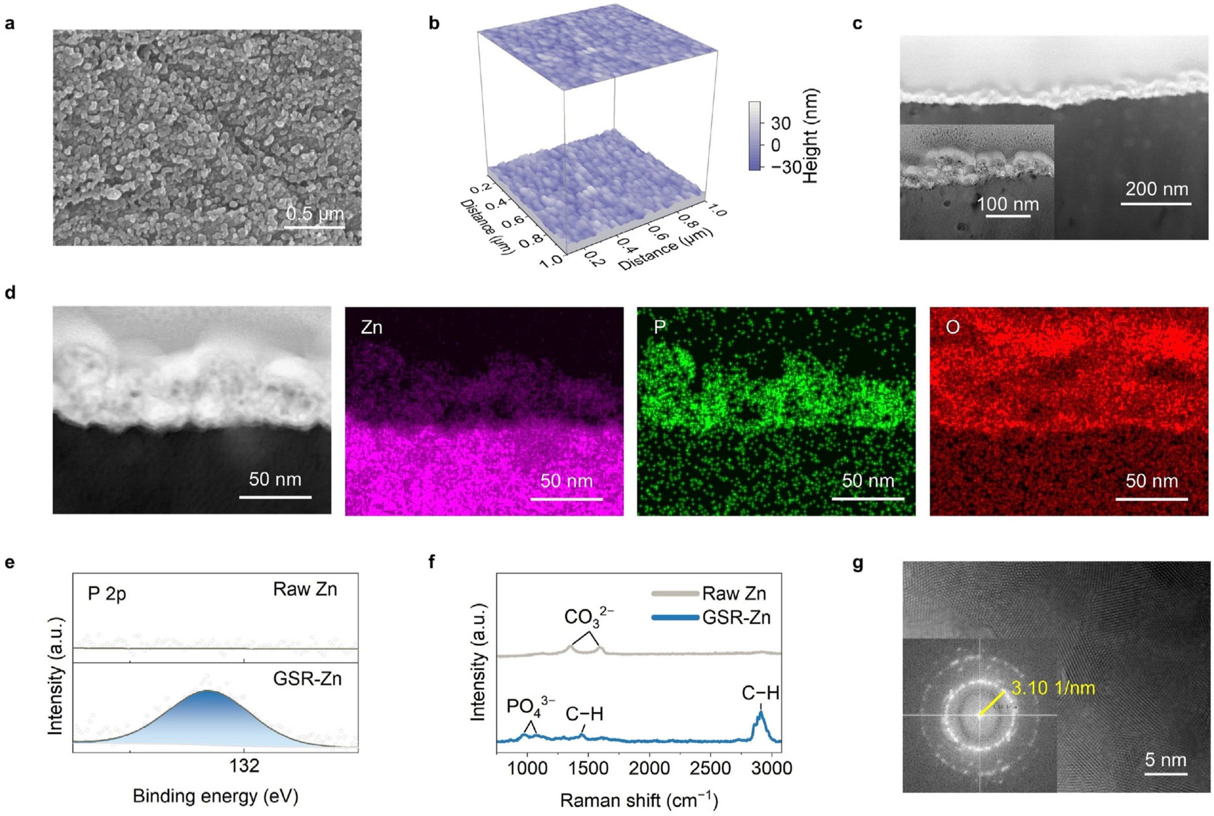

Fig. 2. Characterization of the GSR-Zn. (a) SEM image of the surface morphology. (b) AFM 3D image. (c) Cross-section image. The inset is the TEM image. (d) EDS mapping. (e) XPS spectra. (f) Raman spectra. (g) HR-TEM image. The inset is the fast Fourier transform (FFT) image.

To further demonstrate the superiority of GSR treatment, zinc micro-flakes were selected, and the GSR-treated ones exhibited identical surface morphology to that of zinc metal foils (Fig. S4). Due to the significantly larger specific surface area of the zinc micro-flakes, the test signal during interphase layer characterization was enhanced. The original zinc micro-flakes display obvious diffraction peaks of zinc oxide and basic zinc carbonate (Fig. S5), which disappear after the GSR treatment and are replaced by diffraction peaks of zinc phosphate. XPS analysis also reveals the disappearance of the oxide layer signal and the appearance of P and C signals from zinc phosphate and PVA in the GSR-treated zinc micro-flakes (Fig. S6). This confirms that the GSR treatment can facilitate the formation of uniform zinc phosphate-rich interphase while removing the original surface passivation layer, and it works well for zinc with different morphologies.

2.3. Electrochemical performance of GSR-Zn

After confirming the composition and structure of the zinc phosphate-dominated interphase layer, its impact on zinc performance was investigated. In the chronoamperometry test (Fig. 3a), the GSR-Zn gets into the stable 3D diffusion state in just seconds, while the Raw Zn counterpart is in the 2D diffusion all the time. This is because the zinc phosphate-dominated interphase with a generally distributed active site could greatly shorten the ion transportation distance. As a result, the zinc after GSR treatment can enter the steady diffusion stage in a short time [46,47]. Additionally, like Raw Zn, the GSR-Zn exhibits a nucleation overpotential of 0.030 V but with a much lower zinc plating overpotential (0.020 V), indicating its fast reaction kinetics (Fig. 3b). For the nucleation overpotentials of Polished Zn (0.045 V) and Etched Zn (0.033 V), they are both higher than that of Raw Zn, which can be ascribed to the increased areal density of instantaneous nucleation by the abundant defects created by mechanical polishing and the porous structure resulting from acid etching [48–50]. After this, LSV curves and Tafel plots were obtained to demonstrate the ability of GSR-Zn to resist the corrosion. As shown in Fig. 3c and Fig. S7, the GSR-Zn exhibits the lowest HER onset potential and corrosion current, which can be attributed to the well-constructed zinc phosphate-dominated interphase layer that has relatively smooth morphology, electronic insulation, ionic conductivity ability, and relatively moderate hydrophilicity (Fig. S8). In contrast, the Polished Zn and Etched Zn without any protective layer display exacerbated corrosion reactions compared to the Raw Zn.

In the long cycling test (Fig. 3d), the Raw Zn experiences short circuits within 71 cycles due to the local dendritic growth piercing the separator. The vigorous hydrogen evolution-induced corrosion reaction for Polished Zn makes it exhibit an even shorter lifetime than Raw Zn. Since acid etching creates numerous pores in the Etched Zn, they could initially behave as preferential sites for zinc deposition,

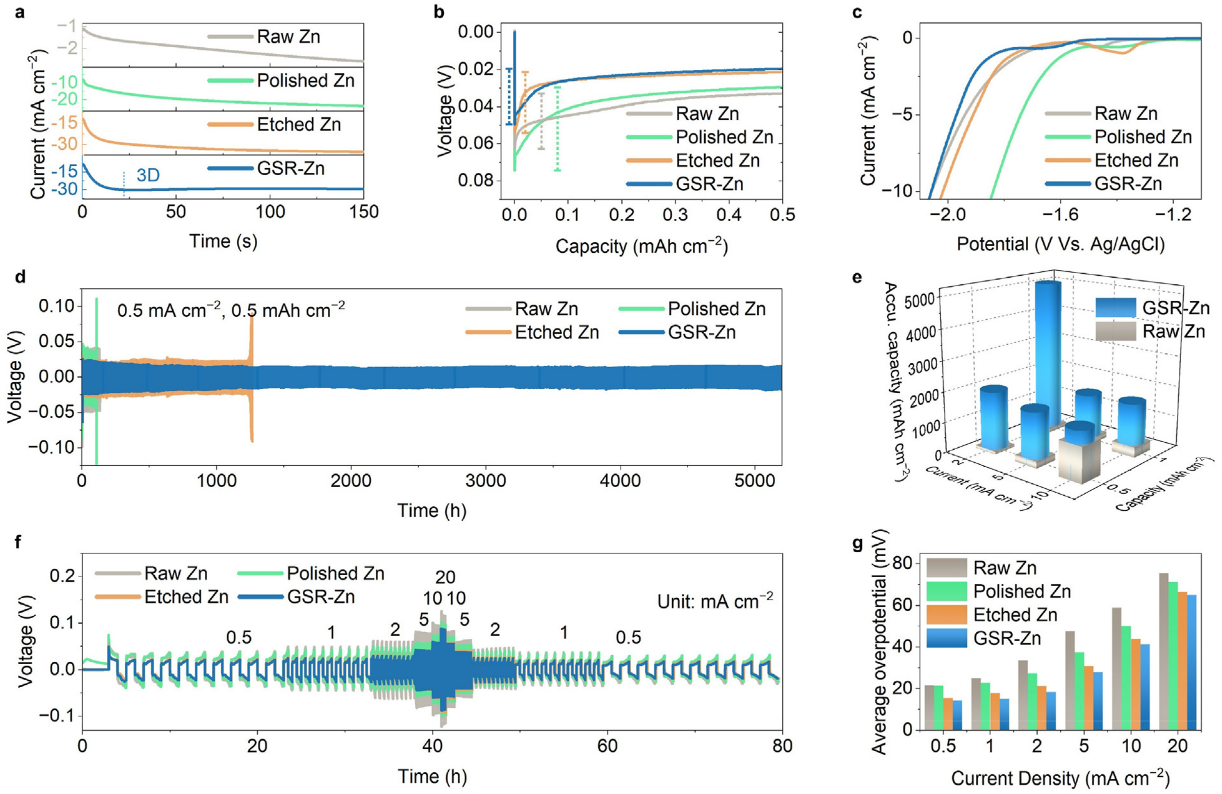

Fig. 3. Performance of zinc electrodes with and without treatment. (a) Chronoamperometry (CA) curves with an applied voltage of 0.15 V. (b) Voltage-time curves at 0.5 mA cm^{-2}. (c) Linear sweep voltammetry (LSV) curves in 0.5 mol L^{-1} Na_2SO_4. (d) Long-term cycling performance of symmetrical Zn cells at 0.5 mA cm^{-2} and 0.5 mAh cm^{-2}. (e) Cumulative capacity statistics for symmetrical Zn cells. (f) Rate performance of symmetrical Zn cells. (g) Overpotential statistics at different current densities.

showing some improvement in cycle life over Raw Zn. However, the Etched Zn eventually fails because of the uneven zinc deposition and side reactions. Thanks to the uniform removal of the surface passivation layer and in situ construction of an artificial interphase layer for rapid zinc ion conduction and inhibition of corrosion reaction, the GSR-Zn delivers the most extended cycle life of 2600 cycles at 0.5 mA cm^{-2} and 0.5 mAh cm^{-2}. Furthermore, it also demonstrates excellent cycling stability at increased current densities or capacities. At 2 mA cm^{-2} and 1 mAh cm^{-2}, the cumulative cycling capacity of the GSR-Zn symmetric battery can reach 5059 mAh cm^{-2} (Fig. 3e and Fig. S9). Additionally, the GSR-Zn also exhibits superior rate capability with constantly lowest overpotential among the four kinds of zinc electrodes at the selected current densities (Fig. 3f and g). As a comparison, ex situ zinc phosphate coating was introduced to the zinc surface as a control group [51]. The reaction time was controlled within a few seconds to obtain amorphous zinc phosphate (Fig. S10). After this, the amorphous zinc phosphate was mixed with PVA to form a slurry and spin-coated to the polished zinc surface with a coating thickness below 10 μm (Fig. S11). Compared to GSR-Zn, the zinc with ex situ phosphate coating manifests higher overpotentials and inferior cycling stability in symmetrical cells (Fig. S12). The above results demonstrate the advantages of GSR treatment in transforming the native passivation layer into a thin and uniform composite interphase layer for facilitating fast zinc ion transport and inhibiting H_2 evolution, consequently significantly enhancing the cyclic stability of zinc electrodes.

2.4. DFT calculations to reveal the benefits of the zinc phosphate-dominated interphase

Density functional theory (DFT) calculations were conducted to further elucidate the impact of the designed interphase layer on the zinc deposition process. After careful consideration, three systems were modeled: Zn, ZnO@Zn, and PVA@ZPO@Zn, and the adsorption energies of zinc toward these zinc surfaces were calculated (Fig. 4a and b). For PVA@ZPO@Zn, considering the minimal steric hindrance of the PVA network for zinc ion transport, the interface between PVA and ZPO was chosen as the computational site [52,53]. The adsorption energy of Zn on the bare zinc, ZnO, and ZPO are −2.32 eV, −2.55 eV, and −3.11 eV (Fig. 4b), respectively, among which the ZPO has the strongest adsorption energy towards the Zn atoms, that is, the highest affinity for zinc. ZnO also exhibits a slightly stronger adsorption energy than bare zinc, suggesting that affinity is only one of the factors determining the electrochemical performance of zinc. To this end, the diffusion ability of ions in the bulk phase of ZnO and ZPO was calculated. Phosphate compounds have been confirmed to perform well in the diffusion of zinc ions [30,54,55]. Along the *c* axis of ZPO, channels for quick transportation of zinc ions are provided (Fig. 4c), which can diffuse zinc ions in a

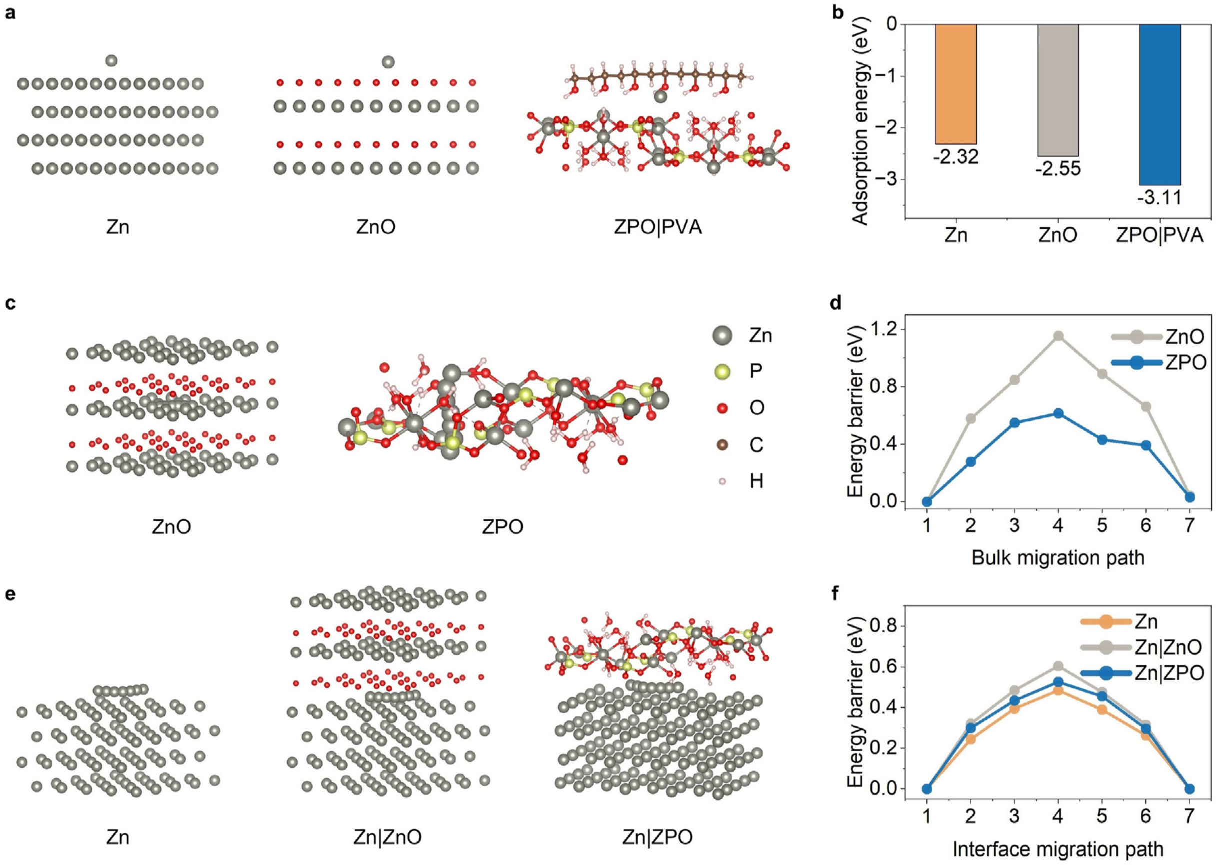

Fig. 4. DFT calculations. (a) Modelling of Zn adsorption on the surface of zinc electrodes. (b) Adsorption energy of zinc atoms on the surface of zinc electrodes. (c) Modelling of zinc diffusion in the bulk phase of ZnO and ZPO. (d) Diffusion energy barrier of zinc in the bulk phase of ZnO and ZPO. (e) Modelling of zinc diffusion at the material interfaces. (f) Diffusion energy barrier of zinc at the material interface.

fast manner to avoid the dendrite growth triggered by insufficient localized zinc ion concentration [31,56]. As a result, the ZPO has a lower bulk-phase Zn^{2+} diffusion energy barrier than the ZnO (0.62 vs. 1.16 eV, Fig. 4d). Additionally, since the lateral diffusion of zinc ions is another critical factor in configuring uniform zinc deposition [57], the zinc diffusion at the Zn, ZnO@Zn, and PVA@ZPO@Zn surface or interface was also calculated. As indicated in Fig. 4e and f, the zinc diffusion energy barrier at the material surface or interface follows the order of bare zinc < ZPO < ZnO, suggesting that the ZPO has an advantage over ZnO in promoting uniform zinc deposition. The strong zinc adsorption energy and small zinc diffusion energy barrier in bulk and interface make PVA@ZPO a powerful interphase with significantly improved stability.

2.5. Deposition behavior of the zinc with and without GSR treatment

After getting the calculated results, the deposition behavior of zinc with and without GSR treatment was investigated. The SEM images clearly show the strong contrast between the two kinds of zinc electrodes after 100 cycles at 0.5 mA cm^{-2} and 0.5 mAh cm^{-2} (Fig. 5a and c). For a microscopic area, the Raw Zn tends to have an uncertainty and random distribution of zinc dendrite growth because of a passivation layer. The zoom-out image (inset in Fig. 5a) shows a more intuitive and visual result with excessive zinc only deposited in some areas. In contrast, after removing the passivation layer, the GSR-Zn produces a composite interphase layer with high zinc ion adsorption and diffusion ability that effectively regulates the zinc with homogeneous reactivity in the whole electrode region and consequently realizes dendrite-free zinc deposition (Fig. 5c). In situ optical microscopy was further carried out to observe the real-time deposition behavior of Raw Zn and GSR-Zn (Fig. 5b and d). For Raw Zn, the presence of a passivation layer leads to localized deposition of zinc, and accordingly, there is obvious zinc dendrite growth as the deposition capacity increases (Fig. 5b). Moreover, the zinc also preferentially deposits on the cross-section of Raw Zn due to the freshly exposed zinc surface without a passivation layer. Different from Raw Zn, the zinc phosphate-dominated interphase on the GSR-Zn can effectively regulate the zinc deposition process, resulting in uniform deposition of zinc in the whole plating process (Fig. 5d).

COMSOL Multiphysics was then conducted to investigate the distribution of dendrites and ion concentration during zinc deposition on Raw Zn and GSR-Zn. It is clear that the surface scratches on the Raw zinc induce the inhomogeneous distribution of Zn^{2+} and current density (Fig. 5e and Figs. S13a and c)

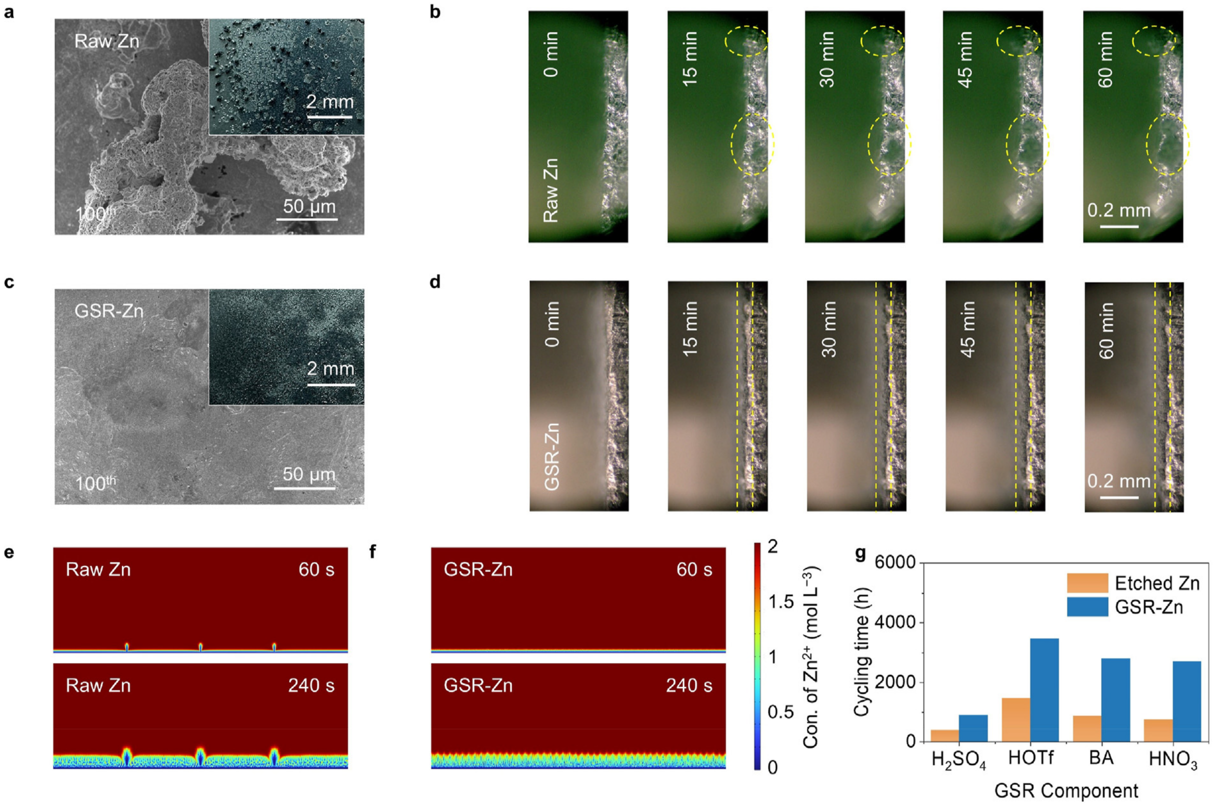

Fig. 5. Depositional behavior of zinc. (a, c) SEM images of the Zn electrodes after 100 cycles at 0.5 mA cm^{-2} and 0.5 mAh cm^{-2}. Raw Zn (a) and GSR-Zn (c). The insets are the macro photos of the Zn electrodes. (b, d) Cross-section optical photos at a plating current density of 1 mA cm^{-2} for 1 h. Raw Zn (b) and GSR-Zn (d). (e, f) Distribution of Zn^{2+} concentration during the zinc deposition process simulated by COMSOL. Raw Zn (e) and GSR-Zn (f). (g) Cycle time statistics of symmetric batteries with the zinc electrodes after different acid treatments.

and consequently result in obvious dendrite growth. In contrast, the GSR-Zn possesses uniform surface morphology and homogeneous ion diffusion ability, leading to homogeneous ion and current density distribution on the electrode surface to suppress the occurrence of dendrite growth [58,59]. It is worth mentioning that the GSR treatment is simple to operate and has the potential for large-scale production of high-performance zinc electrodes. For example, we have designed a scale-up device to treat a Zn foil with a length of 50 cm (Fig. S14). Additionally, the versatility of the GSR method was demonstrated by using

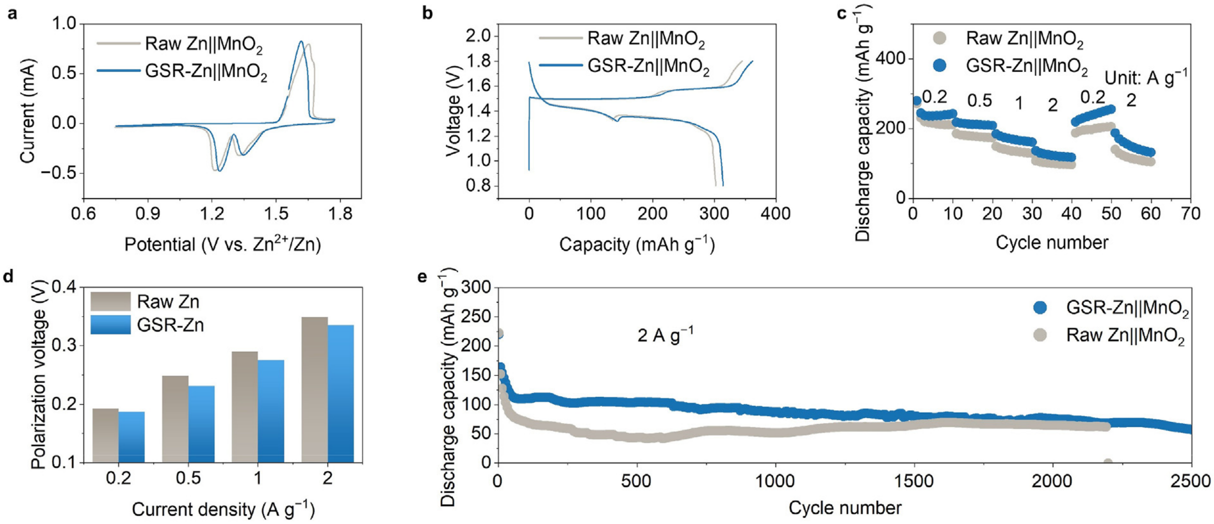

Fig. 6. Performance of the Zn||MnO_2 cells. (a) Cyclic voltammetry. (b) Charge/Discharge profiles. (c) Rate performance. (d) Statistics of the polarization voltage at different current densities. (e) Long cycle tests.

different acids as the sustained-release components, like sulfuric acid (H_2SO_4), trifluoromethanesulfonic acid (HOTf), benzenesulfonic acid (BA), trifluoromethanesulfonic acid (HOTf), and nitric acid (HNO_3). It can be seen from Figs. S15a–d that samples etched with aqueous solutions of sulfuric acid, benzenesulfonic acid, and trifluoromethanesulfonic acid exhibit pronounced porous morphologies, while the one treated by nitric acid solution results in a thick layer of nanosheet-like hydroxylated zinc nitrate. Since the GSR treatment can effectively regulate the interfacial reaction between the acid and zinc, the GSR-treated samples show smooth surfaces (Figs. S15e–h) and demonstrate significantly longer cycle life in symmetric cells when compared to the samples treated with aqueous acid solutions (Fig. 5g and Fig. S16). This provides solid evidence that the GSR method is a simple and versatile strategy that can effectively enhance the stability of zinc electrodes and is easy to scale up.

2.6. Full cell performance

For aqueous zinc batteries, the uniformity of zinc deposition on the anode and its ability to suppress side reactions directly determine the electrochemical performance of full batteries, like lifetime, reversible capacity, rate capability, etc [60]. In this consideration, batteries using MnO_2 as the cathode (Rod-shaped α-MnO_2, Fig. S17) were assembled to check whether the superiority of GSR-Zn can be well maintained under the full battery working environment. In cyclic voltammetry (CV) curves (Fig. 6a), the two pairs of peaks is recognized to involve the co-insertion of H^+ and Zn^{2+} into the α-MnO_2 [61–63]. Due to the decreased plating/stripping overpotential of GSR-Zn, the GSR-Zn-based full cells exhibit narrower gaps between the redox peaks and deliver larger reversible capacity (Fig. 6b) than the cells with Raw Zn anode. Besides, the improved electrode kinetics of the GSR-Zn also make the full cell realize acceptable rate capability with decent capacity decrease and polarization voltage increase as the enlargement of the current density (Fig. 6c and d). Moreover, since the zinc phosphate-dominated interphase layer can effectively inhibit the dendrite growth and side reactions of GSR-Zn during long cycle test, the GSR-Zn-based full cells achieve a lifetime of over 2500 cycles, longer than the Raw Zn-based cells (2197 cycles, Fig. 6d). Apparently, the improved stability and reaction kinetics of GSR-Zn can be well preserved in the full cells to promote cell performance.

3. Conclusions

In summary, we have designed a facile and versatile GSR method to address the issue of native passivation layer induced local reactivity of zinc anodes in aqueous zinc batteries. The GSR treatment can in situ convert the original passivation layer into a thin and uniform zinc phosphate-dominated composite interphase layer on the zinc surface. Compared with the traditional passivation layer removing methods that are accompanied by the inevitable introduction of new surface defects, like physical polishing and acid etching, the GSR treatment generated functional interphase layer can realize full protection of zinc anodes with improved zinc ion adsorption and diffusion ability and mitigated corrosion reactions, suppressing the dendrite growth and prolonging the cycling stability in both symmetrical and full cells. In addition, this method also offers advantages such as low processing cost, ease of operation, versatility, and scalability. Our findings provide a new solution for enhancing the performance of aqueous zinc batteries and offer insights for research in optimizing the surface treatment of metal anodes.

CRediT authorship contribution statement

Zi-Long Xie: Conceptualization, Methodology, Investigation, Writing – original draft. **Yunhai Zhu:** Writing – review & editing. **Jia-Yi Du:** Formal analysis. **Dong-Yue Yang:** Visualization. **Hao Chen:** Investigation. **Zhi Wang:** Investigation. **Gang Huang:** Writing – review & editing, Supervision, Funding acquisition. **Xin-Bo Zhang:** Supervision, Project administration, Funding acquisition.

Declaration of competing interest

The authors declare that they have no competing financial interests or personal relationships that could have appeared to influence the work reported in this paper.

Acknowledgements

This work was financially supported by the National Key R&D Program of China (Grant 2022YFB2402200), National Natural Science Foundation of China (Grant 92372206, 52271140, 52171194), Jilin Province Science and Technology Development Plan Funding Project (Grant YDZJ202301-ZYTS545), National Natural Science Foundation of China Excellent Young Scientists (Overseas), and Youth Innovation Promotion Association CAS (Grant 2020230). The authors thank HUASUAN Technology Co. Ltd. for the technical support on theoretical calculations. The authors thank Dr. Yong-Lai Zhang for the valuable discussions.

Appendix A. Supplementary data

Supplementary data to this article can be found online at https://doi.org/10.1016/j.gee.2025.02.004.

References

[1] C. Li, S. Jin, L.A. Archer, L.F. Nazar, Joule 6 (2022) 1733–1738.
[2] Y. Cheng, L. Luo, L. Zhong, J. Chen, B. Li, W. Wang, S.X. Mao, C. Wang, V.L. Sprenkle, G. Li, J. Liu, ACS Appl. Mater. Interfaces 8 (2016) 13673–13677.
[3] W. Li, K. Wang, S. Cheng, K. Jiang, Adv. Energy Mater. 9 (2019) 1900993.
[4] Y. Shang, D. Kundu, Joule 7 (2023) 244–250.
[5] J. Zheng, D.C. Bock, T. Tang, Q. Zhao, J. Yin, K.R. Tallman, G. Wheeler, X. Liu, Y. Deng, S. Jin, A.C. Marschilok, E.S. Takeuchi, K.J. Takeuchi, L.A. Archer, Nat. Energy 6 (2021) 398–406.

[6] Q. Zhang, P. Zhi, J. Zhang, S. Duan, X. Yao, S. Liu, Z. Sun, S.C. Jun, N. Zhao, L. Dai, L. Wang, X. Wu, Z. He, Q. Zhang, Adv. Mater. 36 (2024) 2313152.
[7] T. Wang, P. Wang, L. Pan, Z. He, L. Dai, L. Wang, S. Liu, S.C. Jun, B. Lu, S. Liang, J. Zhou, Adv. Energy Mater. 13 (2023) 2203523.
[8] X. Gu, Y. Du, X. Ren, F. Ma, X. Zhang, M. Li, Q. Wang, L. Zhang, C. Lai, S. Zhang, Adv. Funct. Mater. 34 (2024) 2316541.
[9] J. Hao, B. Li, X. Li, X. Zeng, S. Zhang, F. Yang, S. Liu, D. Li, C. Wu, Z. Guo, Adv. Mater. 32 (2020) 2003021.
[10] H.J. Kim, S. Kim, K. Heo, J.-H. Lim, H. Yashiro, S.-T. Myung, Adv. Energy Mater. 13 (2023) 2203189.
[11] Z. Wu, J. Zou, Y. Li, E.J. Hansen, D. Sun, H. Wang, L. Wang, J. Liu, Small 19 (2023) 2206634.
[12] Y. Zhang, X. Han, R. Liu, Z. Yang, S. Zhang, Y. Zhang, H. Wang, Y. Cao, A. Chen, J. Sun, Small 18 (2022) 2105978.
[13] X. Wang, J. Meng, X. Lin, Y. Yang, S. Zhou, Y. Wang, A. Pan, Adv. Funct. Mater. 31 (2021) 2106114.
[14] P. Wang, B. Sun, X. Wei, L. Yang, H. Wu, Chem. Eng. J. 455 (2023) 140827.
[15] S. Higashi, S.W. Lee, J.S. Lee, K. Takechi, Y. Cui, Nat. Commun. 7 (2016) 11801.
[16] Z. Cai, J. Wang, Y. Sun, eScience 3 (2023) 100093.
[17] Y. Xiong, X. Gu, Z. Liu, X. Ren, Y. Jiang, H. Xu, L. Zhuo, G. Jiang, J. Colloid Interface Sci. 662 (2024) 604–613.
[18] B. Li, P. Ruan, X. Xu, Z. He, X. Zhu, L. Pan, Z. Peng, Y. Liu, P. Zhou, B. Lu, L. Dai, J. Zhou, Nano-Micro Lett. 16 (2024) 76.
[19] Q. Wang, B.-H. Xu, Y.-X. Du, L.-Y. Kuang, Z.-S. Lin, X.-X. Gu, Rare Met. 44 (2025) 209–217.
[20] P. Qiu, D. Persson, C. Leygraf, J. Electrochem. Soc. 156 (2009) C81.
[21] P. He, J. Huang, ACS Energy Lett. 6 (2021) 1990–1995.
[22] G. Lee, Y. Lee, S. Kim, D. Kim, H. Park, M. Woo, T. Song, U. Paik, Sci. Rep. 13 (2023) 22847.
[23] D. Liu, Z. Zhang, J. Feng, Z. Yu, F. Meng, C. Shi, G. Xu, S. Shi, W. Liu, Colloids Surf. A Physicochem. Eng. Asp. 656 (2023) 130500.
[24] W. Vijselaar, P. Westerik, J. Veerbeek, R.M. Tiggelaar, E. Berenschot, N.R. Tas, H. Gardeniers, J. Huskens, Nat. Energy 3 (2018) 185–192.
[25] H. Park, H. Seo, S.E. Kim, Sci. Rep. 10 (2020) 21720.
[26] C. Yuan, L. Yin, P. Du, Y. Yu, K. Zhang, X. Ren, X. Zhan, S. Gao, Chem. Eng. J. 442 (2022) 136231.
[27] H. Peng, Y. Fang, J. Wang, P. Ruan, Y. Tang, B. Lu, X. Cao, S. Liang, J. Zhou, Matter 5 (2022) 4363–4378.
[28] X. He, Y. Cui, Y. Qian, Y. Wu, H. Ling, H. Zhang, X.-Y. Kong, Y. Zhao, M. Xue, L. Jiang, L. Wen, J. Am. Chem. Soc. 144 (2022) 11168–11177.
[29] M. Wang, Y. Meng, K. Li, T. Ahmad, N. Chen, Y. Xu, J. Sun, M. Chuai, X. Zheng, Y. Yuan, C. Shen, Z. Zhang, W. Chen, eScience 2 (2022) 509–517.
[30] W. Shin, J. Lee, Y. Kim, H. Steinfink, A. Heller, J. Am. Chem. Soc. 127 (2005) 14590–14591.
[31] X. Zeng, J. Mao, J. Hao, J. Liu, S. Liu, Z. Wang, Y. Wang, S. Zhang, T. Zheng, J. Liu, P. Rao, Z. Guo, Adv. Mater. 33 (2021) 2007416.
[32] Y. Zhou, J. Li, Y. Zhang, D. Dong, E. Zhang, F. Ji, Z. Qin, J. Yang, F. Yao, J. Phys. Chem. B 121 (2017) 800–814.
[33] C.P. Goodrich, M.P. Brenner, K. Ribbeck, Nat. Commun. 9 (2018) 4348.
[34] E. Axpe, D. Chan, G.S. Offeddu, Y. Chang, D. Merida, H.L. Hernandez, E.A. Appel, Macromolecules 52 (2019) 6889–6897.
[35] F. Ai, Z. Wang, N.-C. Lai, Q. Zou, Z. Liang, Y.-C. Lu, Nat. Energy 7 (2022) 417–426.
[36] Y. Wang, T. Wang, D. Dong, J. Xie, Y. Guan, Y. Huang, J. Fan, Y.-C. Lu, Matter 5 (2022) 162–179.
[37] Z. Xing, Y. Sun, X. Xie, Y. Tang, G. Xu, J. Han, B. Lu, S. Liang, G. Chen, J. Zhou, Angew. Chem. Int. Ed. 62 (2023) e202215324.
[38] S. Zhang, M. Ye, Y. Zhang, Y. Tang, X. Liu, C.C. Li, Adv. Funct. Mater. 33 (2023) 2208230.
[39] J. Winiarski, W. Tylus, K. Winiarska, I. Szczygieł, B. Szczygieł, J. Spectrosc. 2018 (2018) e2079278.
[40] A. Kaleva, T. Tassaing, V. Saarimaa, G. Le Bourdon, P. Väisänen, A. Markkula, E. Levänen, Corros. Sci. 174 (2020) 108850.
[41] Y. Zhang, P.C. Zhu, D. Edgren, J. Polym. Res. 17 (2010) 725–730.
[42] Y. Chen, Z. Wang, X. Li, X. Yao, C. Wang, Y. Li, W. Xue, D. Yu, S.Y. Kim, F. Yang, A. Kushima, G. Zhang, H. Huang, N. Wu, Y.-W. Mai, J.B. Goodenough, J. Li, Nature 578 (2020) 251–255.
[43] X.-R. Chen, Y.-X. Yao, C. Yan, R. Zhang, X.-B. Cheng, Q. Zhang, Angew. Chem. Int. Ed. 59 (2020) 7743–7747.
[44] Y. Li, G. Yang, C. Zhang, W.Y. Lieu, C.Y.J. Lim, S. Sun, J. Wang, S. Jiang, Z. Xing, Z. Sofer, M. Ng, W. Liu, Z.W. Seh, Adv. Funct. Mater. 33 (2023) 2210639.
[45] S. Bach, V.R. Celinski, M. Dietzsch, M. Panthöfer, R. Bienert, F. Emmerling, J.S. auf der Günne, W. Tremel, J. Am. Chem. Soc. 137 (2015) 2285–2294.
[46] M. Zhou, S. Guo, J. Li, X. Luo, Z. Liu, T. Zhang, X. Cao, M. Long, B. Lu, A. Pan, G. Fang, J. Zhou, S. Liang, Adv. Mater. 33 (2021) 2100187.
[47] K. Xie, K. Ren, Q. Wang, Y. Lin, F. Ma, C. Sun, Y. Li, X. Zhao, C. Lai, eScience 3 (2023) 100153.
[48] A. Pei, G. Zheng, F. Shi, Y. Li, Y. Cui, Nano Lett. 17 (2017) 1132–1139.
[49] X. Gao, Y.-N. Zhou, D. Han, J. Zhou, D. Zhou, W. Tang, J.B. Goodenough, Joule 4 (2020) 1864–1879.
[50] M. Pise, M. Muduli, A. Chatterjee, B.P. Kashyap, R.N. Singh, S.S.V. Tatiparti, Results Surf. Interfaces 6 (2022) 100044.
[51] D. Li, Y. Tang, S. Liang, B. Lu, G. Chen, J. Zhou, Energy Environ. Sci. 16 (2023) 3381–3390.
[52] L. Han, Y. Guo, F. Ning, X. Liu, J. Yi, Q. Luo, B. Qu, J. Yue, Y. Lu, Q. Li, Adv. Mater. 36 (2024) 2308086.
[53] Z. Guo, L. Fan, C. Zhao, A. Chen, N. Liu, Y. Zhang, N. Zhang, Adv. Mater. 34 (2022) 2105133.
[54] P. Hu, Z. Zou, X. Sun, D. Wang, J. Ma, Q. Kong, D. Xiao, L. Gu, X. Zhou, J. Zhao, S. Dong, B. He, M. Avdeev, S. Shi, G. Cui, L. Chen, Adv. Mater. 32 (2020) 1907526.
[55] Q. Zou, Z. Liang, W. Wang, D. Dong, Y.-C. Lu, Energy Environ. Sci. 16 (2023) 6026–6034.
[56] R. Essehli, H. Ben Yahia, R. Amin, F. El-Mellouhi, I. Belharouak, Energy Storage Mater. 24 (2020) 343–350.
[57] Z. Wu, C. Wang, Z. Hui, H. Liu, S. Wang, S. Yu, X. Xing, J. Holoubek, Q. Miao, H.L. Xin, P. Liu, Nat. Energy 8 (2023) 340–350.
[58] M. Jiao, L. Dai, H. Ren, M. Zhang, X. Xiao, B. Wang, J. Yang, B. Liu, G. Zhou, H. Cheng, Angew. Chem. Int. Ed. 62 (2023) e202301114.
[59] S. Wu, Z. Hu, P. He, L. Ren, J. Huang, J. Luo, eScience 3 (2023) 100120.
[60] J. Zheng, L.A. Archer, Sci. Adv. 7 (2021) eabe0219.
[61] W. Sun, F. Wang, S. Hou, C. Yang, X. Fan, Z. Ma, T. Gao, F. Han, R. Hu, M. Zhu, C. Wang, J. Am. Chem. Soc. 139 (2017) 9775–9778.
[62] H. Yang, W. Zhou, D. Chen, J. Liu, Z. Yuan, M. Lu, L. Shen, V. Shulga, W. Han, D. Chao, Energy Environ. Sci. 15 (2022) 1106–1118.
[63] M. Chuai, J. Yang, M. Wang, Y. Yuan, Z. Liu, Y. Xu, Y. Yin, J. Sun, X. Zheng, N. Chen, W. Chen, eScience 1 (2021) 178–185.